

ARMY RESEARCH LABORATORY



**Innovative Processing of Highly Efficient Rare Earth Free
Magnetocaloric Materials**

by Anit Giri and Kyu Cho

ARL-TR-6866

March 2014

NOTICES

Disclaimers

The findings in this report are not to be construed as an official Department of the Army position unless so designated by other authorized documents.

Citation of manufacturer's or trade names does not constitute an official endorsement or approval of the use thereof.

Destroy this report when it is no longer needed. Do not return it to the originator.

Army Research Laboratory

Aberdeen Proving Ground, MD 21005

ARL-TR-6866

March 2014

Innovative Processing of Highly Efficient Rare Earth Free Magnetocaloric Materials

Anit Giri

Bowhead Science and Technology

Kyu Cho

Weapons and Materials Research Directorate, ARL

REPORT DOCUMENTATION PAGE

Form Approved
OMB No. 0704-0188

Public reporting burden for this collection of information is estimated to average 1 hour per response, including the time for reviewing instructions, searching existing data sources, gathering and maintaining the data needed, and completing and reviewing the collection information. Send comments regarding this burden estimate or any other aspect of this collection of information, including suggestions for reducing the burden, to Department of Defense, Washington Headquarters Services, Directorate for Information Operations and Reports (0704-0188), 1215 Jefferson Davis Highway, Suite 1204, Arlington, VA 22202-4302. Respondents should be aware that notwithstanding any other provision of law, no person shall be subject to any penalty for failing to comply with a collection of information if it does not display a currently valid OMB control number.

PLEASE DO NOT RETURN YOUR FORM TO THE ABOVE ADDRESS.

1. REPORT DATE (DD-MM-YYYY) March 2014		2. REPORT TYPE DRI Final Report		3. DATES COVERED (From - To) 10/1/2011–9/30/2013	
4. TITLE AND SUBTITLE Innovative Processing of Highly Efficient Rare Earth Free Magnetocaloric Materials				5a. CONTRACT NUMBER	
				5b. GRANT NUMBER	
				5c. PROGRAM ELEMENT NUMBER	
6. AUTHOR(S) Anit Giri and Kyu Cho				5d. PROJECT NUMBER	
				5e. TASK NUMBER	
				5f. WORK UNIT NUMBER	
7. PERFORMING ORGANIZATION NAME(S) AND ADDRESS(ES) U.S. Army Research Laboratory ATTN: RDRL-WMM-D Aberdeen Proving Ground, MD 21005				8. PERFORMING ORGANIZATION REPORT NUMBER ARL-TR-6866	
9. SPONSORING/MONITORING AGENCY NAME(S) AND ADDRESS(ES)				10. SPONSOR/MONITOR'S ACRONYM(S)	
				11. SPONSOR/MONITOR'S REPORT NUMBER(S)	
12. DISTRIBUTION/AVAILABILITY STATEMENT Approved for public release; distribution unlimited.					
13. SUPPLEMENTARY NOTES					
14. ABSTRACT In order to fabricate a magnetic cooling system, it is necessary to develop rare earth free polycrystalline magnetocaloric materials (MCMs) with large magnetocaloric effect (MCE). To increase the MCE, we applied an innovative processing technique to manipulate crystallographic alignment in polycrystalline Ni _{2+x} Mn _{1-x} Ga rare-earth free alloys consisting of thermal cycling about the martensite phase transition temperature under a compressive stress. After crystallographic alignment, there was as high as 79% enhancement of the maximum magnetic entropy change for the magnetic field change of 7 T. Texture measurements using neutron diffraction have shown that thermal cycling leads to crystallographic alignment of the easy magnetization axis along the loading direction, which explains the MCE enhancement by up to 79%. Overall, a methodology for enhancing solid state magnetocaloric cooling has been established.					
15. SUBJECT TERMS magnetocaloric, rare earth, Ni, Mn, Ga					
16. SECURITY CLASSIFICATION OF:			17. LIMITATION OF ABSTRACT UU	18. NUMBER OF PAGES 22	19a. NAME OF RESPONSIBLE PERSON Anit Giri
a. REPORT Unclassified	b. ABSTRACT Unclassified	c. THIS PAGE Unclassified			19b. TELEPHONE NUMBER (Include area code) 410-306-0824

Contents

List of Figures	iv
Acknowledgments	v
1. Objective	1
2. Approach	1
3. Results	1
4. Conclusions	8
5. References	9
6. Transitions	10
Distribution List	12

List of Figures

Figure 1. DSC thermogram of Sample with $x = 0.14$ and all other samples (inset; heating cycle).....	2
Figure 2. Neutron diffraction patterns for samples with (a) $x = 0.14$ and (b) $x = 0.16$	3
Figure 3. (a) HRTEM image of sample with $x = 0.14$, illustrating the six superlattice spots between major reflections (7 spots in total) characteristic of 7M modulated structure. (b) HRTEM image of sample with $x=0.16$ showing a non-modulated structure. The zone axis is [111] and the twinning plane is (202) fct martensite.	4
Figure 4. Magnetization vs. temperature plots under an applied magnetic field of 0.01 T.	5
Figure 5. Schematic of the apparatus employed for isobaric thermal cycling to manipulate crystallographic alignment.....	5
Figure 6. Plot of ΔS_M versus temperature for samples with ($x = 0.14$ and ($x = 0.16$) for 7 T magnetic field change before and after crystallographic alignment.	6
Figure 7. Pole figures illustrating preferred orientation of plane normals (poles) with respect to the laboratory axes. The near north pole (RD) refers to the columnar growth direction of austenite grains, while the center (ND) and near 3 o'clock/6 o'clock positions (TD) refer to the equivalent directions perpendicular to the austenite grain growth axis. The mechanical loading (during thermal cycling) and the magnetization axis were both along the columnar growth direction of the prior austenite grains. (a) Prior to thermal cycling showing maximum MRD of 7.17 and (b) after thermal cycling under 20 MPa stress, where now the (110) pole intensity has increased to 15.7 along the loading direction.	7
Figure 8. (a) Tetragonal lattice of bct martensite showing the location of Ni, Mn and Ga atoms. ABC is the (112) twin plane while AD is the [11-1] twin direction. The alternate fct representation is the skeleton shown by green lines, where it may be noted that the equivalent twin system is (101)[10-1]. The c/a ratio of the fct cell, that is in near orientation coincidence with the austenite lattice, is 1.18. The easy magnetization axis is [110] direction in the bct representation or [100] direction in fct description; note the location of Mn atoms that span the easy magnetization axis. (b) Sketch illustrating twin related transformation of the fct martensite unit cell under compressive load. The figure illustrates how a prior [001] direction rotates approximately by 90 degrees under compressive load, such that the easy magnetization [100] direction now aligns along the loading axis. The pole figures of figure 7 confirm this rotation.	8

Acknowledgments

Experimental supports from the National Institute of Standards and Technology (NIST), Gaithersburg, MD (Dr. Robert Shull, Dr. Cindi Dennis, Brigitte Paterson); New Mexico Institute of Mining and Technology Socorro, NM (Prof. Bhaskar Majumdar and Michael McLeod); University of Central Florida (Prof. Yongho Sohn and Le Zhou); Los Alamos National Laboratory (Dr. Sven Vogel); and Pittsburgh Materials Technology, a division of Thermacore, Pittsburgh, PA, are gratefully acknowledged.

INTENTIONALLY LEFT BLANK.

1. Objective

The DRI research objective is to develop highly efficient, rare-earth, free magnetocaloric materials (REF-MCMs) for self-powered personal and mobile magnetic cooling systems for the Future Warfighter and Future Force.

2. Approach

Self-powered personal and mobile magnetic cooling systems require ultra high performance magnetocaloric materials (MCMs) with a very large magnetocaloric effect (MCE) that can operate under low applied magnetic field change at a near ambient temperature. Single crystal MCMs exhibit such properties, but they are extremely difficult to grow and are cost-prohibitive. The DRI research approach is to use innovative processing techniques to manipulate crystallographic alignment in polycrystalline $\text{Ni}_{2+x}\text{Mn}_{1-x}\text{Ga}$ rare-earth free alloys to achieve very large MCE near room temperature, thereby circumventing the need for single crystal alloys.

3. Results

During the DRI research, we have demonstrated that a novel thermomechanical processing technique can be used to enhance MCE—i.e., maximum isothermal magnetic entropy change per unit mass ($(\Delta S_M)_{\text{max}}$) of rare earth free polycrystalline $\text{Ni}_{2+x}\text{Mn}_{1-x}\text{Ga}$ alloys. This was evidenced by as high as a 79% increase of $(\Delta S_M)_{\text{max}}$ for a MCM alloy with nominal composition $\text{Ni}_{2.16}\text{Mn}_{0.86}\text{Ga}$. Notably, ΔS_M is the most common figure of merit (I) to characterize MCE of MCMs. Texture measurements confirm that crystallographic alignment was likely responsible for the enhanced MCE response.

$\text{Ni}_{2+x}\text{Mn}_{1-x}\text{Ga}$ alloys with starting composition $x = 0.08, 0.10, 0.12, 0.14, 0.16, 0.19, 0.22,$ and 0.24 were produced under the identical processing condition of inert gas triple arc melting, followed by ultra high vacuum homogenization at 1273 K for 72 h at 10^{-6} torr. Two samples with $x = 0.14$ and 0.16 were chosen for thorough structural, thermal, magnetic, and magnetocaloric properties characterization to correlate magnetostructural properties and magnetocaloric effect with composition and processing. Of specific importance was the influence of processing on crystallographic alignment, and the latter's effect on magnetocaloric response.

The thermal behavior of the samples was studied by Differential Scanning Calorimetry (DSC; 10 K/min) measurements. Figure 1 shows a typical DSC thermogram of sample with $x = 0.14$, where an endothermic peak is observed, indicating martensite to austenite structural phase transformation during heating. Austenite start and finish temperatures, A_s and A_f , are 313 K and 318 K, respectively. A reverse transition, austenite to martensite, is characterized by an exothermic peak during the cooling cycle. The martensite start (M_s) and finish (M_f) temperatures are 313 K and 308 K, respectively. Similar transformations were observed for other samples, and the inset in figure 1 shows the heating cycle portion of the DSC thermograms of samples with other compositions for comparison. The mean martensite transformation temperature was found to increase with Ni concentration.

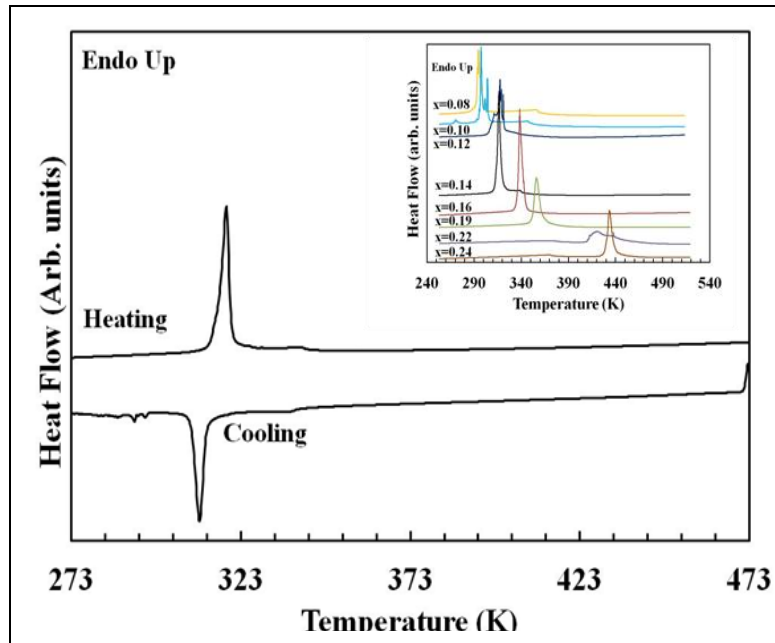


Figure 1. DSC thermogram of Sample with $x = 0.14$ and all other samples (inset; heating cycle).

Figures 2a and b show the neutron diffraction patterns for samples with $x = 0.14$ and $x = 0.16$, respectively. For sample with $x = 0.14$, the GSAS-based Rietveld refinement indicated a 7M modulated monoclinic structure ($I12/m1$) with the lattice parameters: $a = 0.428$ nm, $b = 0.553$ nm, $c = 0.419$ nm, $\alpha = \beta = 90^\circ$, $\gamma = 91.9^\circ$. In the case of $x = 0.16$ sample, the material was found to possess a non-modulated (NM) body-centered tetragonal (bct) structure ($I4/mmm$), with $a = b = 0.387$ nm, $c = 0.648$ nm. Often this structure is referred to with a face-centered tetragonal (fct) lattice that is in near coincidence with the parent austenite phase (fcc, $Fm\bar{3}m$), except that c is extended and a is contracted from the prior austenite Heuslar $L2_1$ structure.

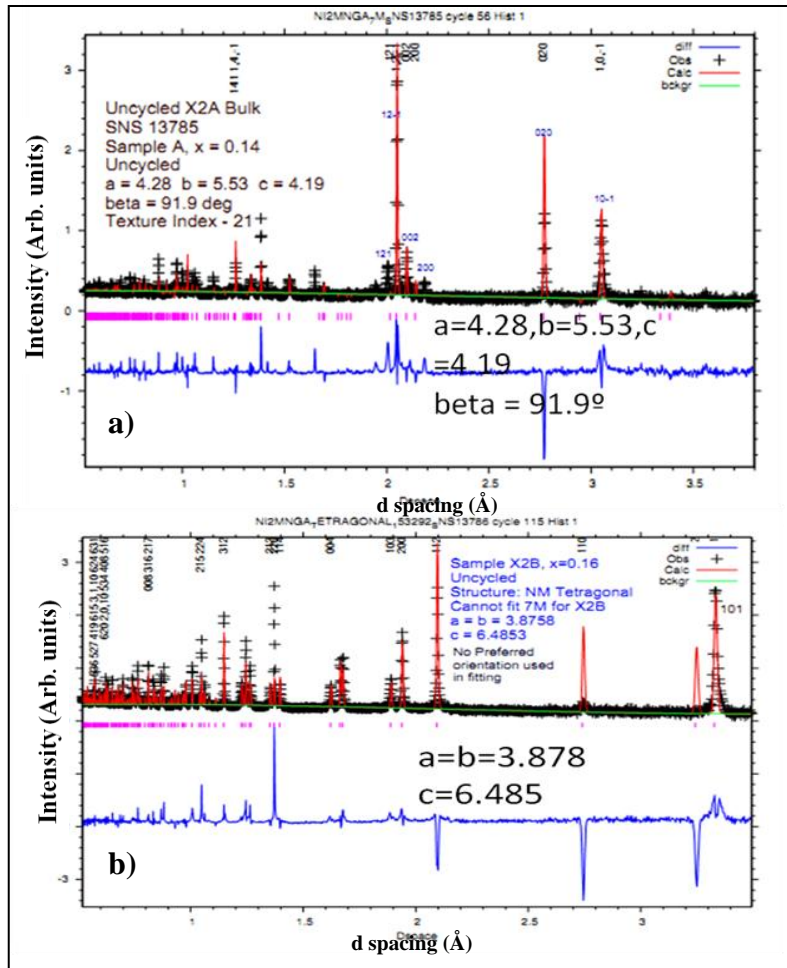


Figure 2. Neutron diffraction patterns for samples with (a) $x = 0.14$ and (b) $x = 0.16$.

Crystal structure analyses using high resolution transmission electron microscopy (HRTEM) are consistent with the results from neutron diffraction experiments. The HRTEM image of figure 3a for $x = 0.14$ shows extensive twinning at multiple length scales in this 7M superstructure, with the minor twins only a few nanometers wide. This type of twinning is characteristic of adaptive martensite, needed to maintain compatibility with the parent face-centered cubic $Fm\bar{3}m$ structure. Fast Fourier transform (FFT) of the minor twins within a major twin in sample $x=0.14$ shows the six superstructure spots characteristic of 7M modulation. The nanoscale twinning is also present for the NM alloy for $x = 0.16$, as shown in figure 3b. The diffraction spots from FFT of twinned location confirms the (101) twinning plane of fct martensite that is in near coincidence with that of {110} austenite.

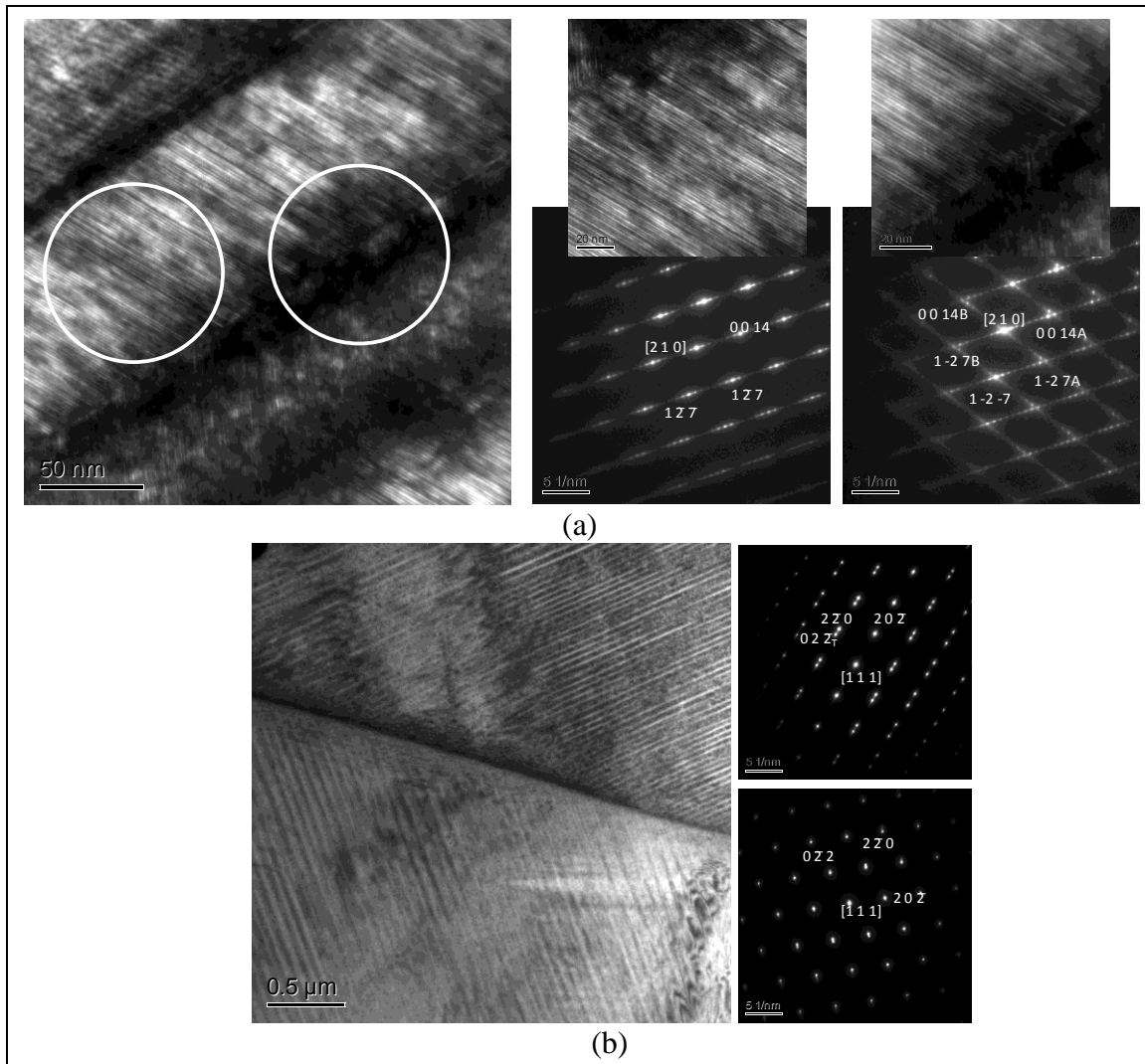


Figure 3. (a) HRTEM image of sample with $x = 0.14$, illustrating the six superlattice spots between major reflections (7 spots in total) characteristic of 7M modulated structure. (b) HRTEM image of sample with $x=0.16$ showing a non-modulated structure. The zone axis is $[111]$ and the twinning plane is (202) fct martensite.

Figure 4 shows the magnetization versus temperature curves for two samples measured under an applied field of 0.01 T (open symbols). The upward jump at 310 K for sample with $x = 0.14$ (open triangle) indicates transformation from martensite to austenite phase. Thereafter, a sudden decrease indicates ferromagnetic to paramagnetic phase transformation at 335 K. For sample B with $x = 0.16$ (open circle), the structural transition appears to occur at or very close to the Curie temperature of 340 K. ΔS_M , which is a measure of MCE, has been calculated from the isothermal magnetization curves, and is presented in figure 6 (open symbols). Sample $x = 0.14$ (open triangle) has a maximum ΔS_M or MCE of $16 \text{ Jkg}^{-1}\text{K}^{-1}$ at 315 K, for an applied field change of 7 T. For the sample with $x = 0.16$ (open circle), with slightly higher Ni content, the MCE increased to $24 \text{ Jkg}^{-1}\text{K}^{-1}$ at 336 K, again for an applied field change of 7 T. The increase in

$(\Delta S_M)_{\max}$ for sample $x = 0.16$ could be ascribed to the simultaneous occurrence of structural and magnetic phase transition at 336 K.

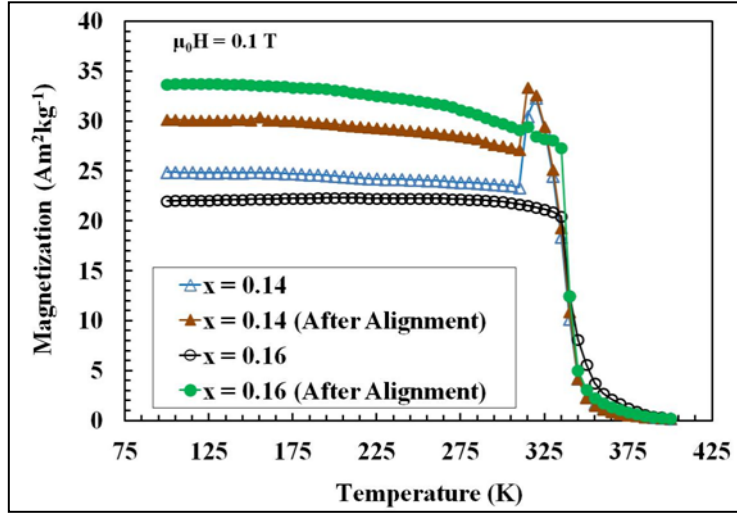


Figure 4. Magnetization vs. temperature plots under an applied magnetic field of 0.01 T.

In order to manipulate crystallographic alignment, constant stress thermal cycling was performed on the samples using an apparatus shown in figure 5. Cubic samples ($\sim 5 \text{ mm}^3$) were thermally cycled 10 times between 298 K and 363 K under a compressive stress of 20 MPa. Figure 4 shows the plots of magnetization versus temperature for the samples after thermomechanical cycling, where the magnetic field was applied along the compressive loading directions. The cycling resulted in enhancements of 56% and 79% of $(\Delta S_M)_{\max}$ for samples with $x = 0.14$ and $x = 0.16$, respectively, as shown in figure 6 (filled symbols).

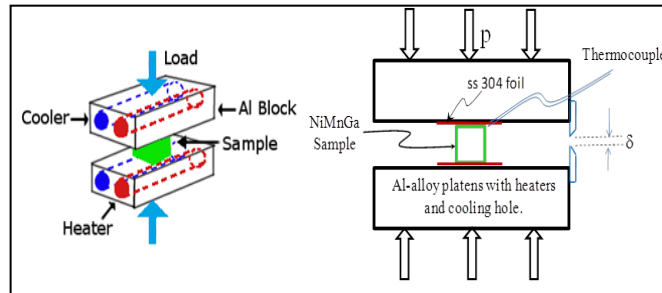


Figure 5. Schematic of the apparatus employed for isobaric thermal cycling to manipulate crystallographic alignment.

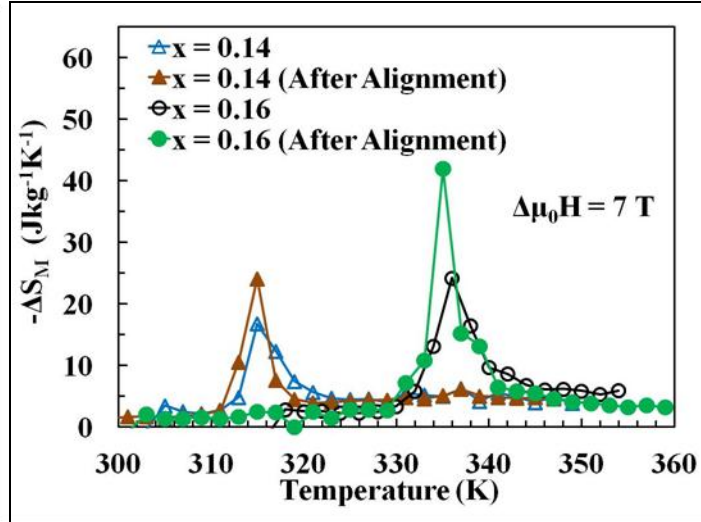


Figure 6. Plot of ΔS_M versus temperature for samples with ($x = 0.14$ and ($x = 0.16$) for 7 T magnetic field change before and after crystallographic alignment.

In order to establish the reason for large MCE enhancement as a result of constant stress thermal cycling, texture measurements were carried out using neutron diffraction in the HIPPO apparatus at the Los Alamos National Laboratories (LANL). Neutron diffraction permitted data to be collected from our entire 5 mm cube samples, rather than being limited to surface layers as would occur if X-ray diffraction were used. Here we focus attention on sample X5-D that was martensite at room temperature, and had identical phase transformation temperatures and non-modulated crystal structure as sample, with $x = 0.16$ that was earlier discussed.

Figure 7 shows the pole figures for sample X5-D before and after thermal cycling under constant stress of 20 MPa. The laboratory axes are explained in the figure caption and represent the preferred orientation of bct martensite phase with respect to this laboratory geometric frame of the samples. Figure 7a shows that before the constant stress thermal cycling, the (110) plane normals (poles) of bct martensite are aligned somewhat along the columnar direction of the austenite grains. The (002) poles (i.e., the longer c -direction of the tetragonal cell) also show some intensity along the columnar direction and a weaker intensity perpendicular to the columnar axis (equatorial zone). The intensities are multiples of random intensity, and the maximum value is 7.18 in this pole figure set. Figure 7b shows that following constant stress thermal cycling along the columnar growth direction of austenite grains, the intensity of the martensite (110) pole has increased to 15.7 along the loading axis (near 12:00 direction). Correspondingly, the intensity of the (200) poles has decreased at the north pole, while it has intensified along the equatorial belt, i.e., perpendicular to the columnar growth direction. The rest of the pole figures in figure 7 are consistent with this description of preferred orientation of martensite variants.

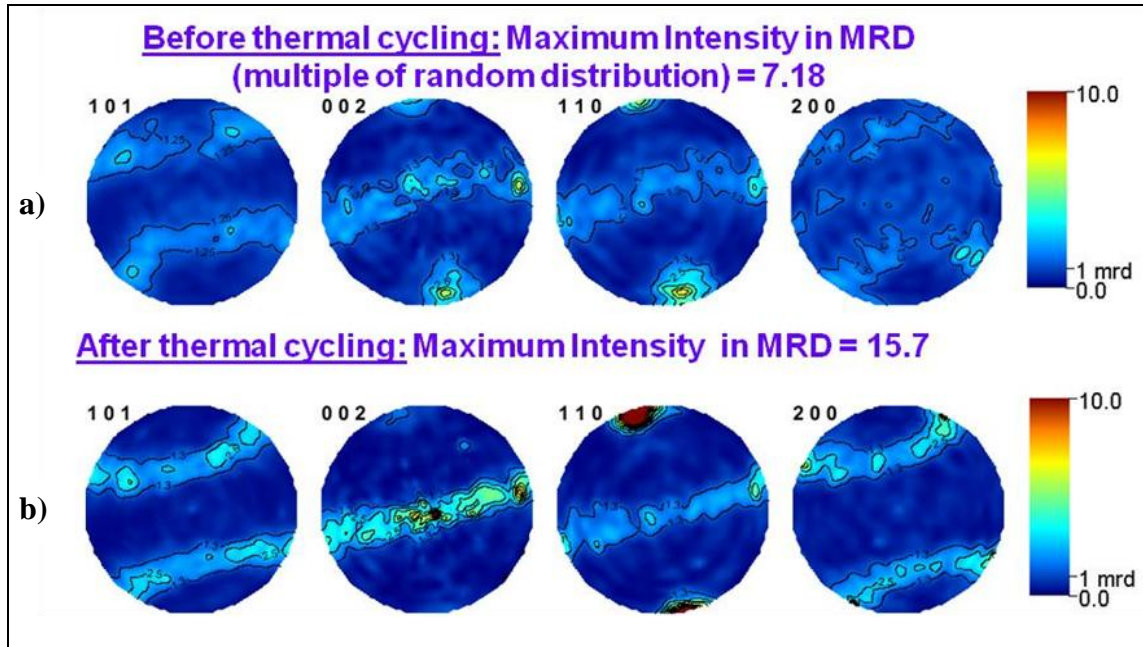


Figure 7. Pole figures illustrating preferred orientation of plane normals (poles) with respect to the laboratory axes. The near north pole (RD) refers to the columnar growth direction of austenite grains, while the center (ND) and near 3 o'clock/6 o'clock positions (TD) refer to the equivalent directions perpendicular to the austenite grain growth axis. The mechanical loading (during thermal cycling) and the magnetization axis were both along the columnar growth direction of the prior austenite grains. (a) Prior to thermal cycling showing maximum MRD of 7.17 and (b) after thermal cycling under 20 MPa stress, where now the (110) pole intensity has increased to 15.7 along the loading direction.

Figure 7 confirms that thermal cycling under compressive load, indeed, leads to crystallographic alignment of the short [100] fct martensite lattice along the loading direction. The twin mechanism is illustrated using the sketches shown in figure 8, where it is shown how a [002] axis under compressive load is transformed to a [100] fct direction, which is also the easy magnetization axis for this tetragonal structure. This crystallographic alignment, thus, explains the significant enhancement of MCE of the sample with $x = 0.16$. A similar texture analysis of the 7M modulated structure is anticipated to show a similar behavior, since it has been observed in single crystal magnetic shape memory alloys (MSMA) of Ni_2MnGa composition. Such experiments on polycrystals need to be conducted in the future. Finally, it may be noted that repeated cycling may also influence twin mobility, as has been observed in single crystal MSMA materials in terms of reduction of twinning stress. The specific heat data in this work provide some insight on this behavior, although additional experiments are needed to shed insight on the role of twin mobility on MCE effect.

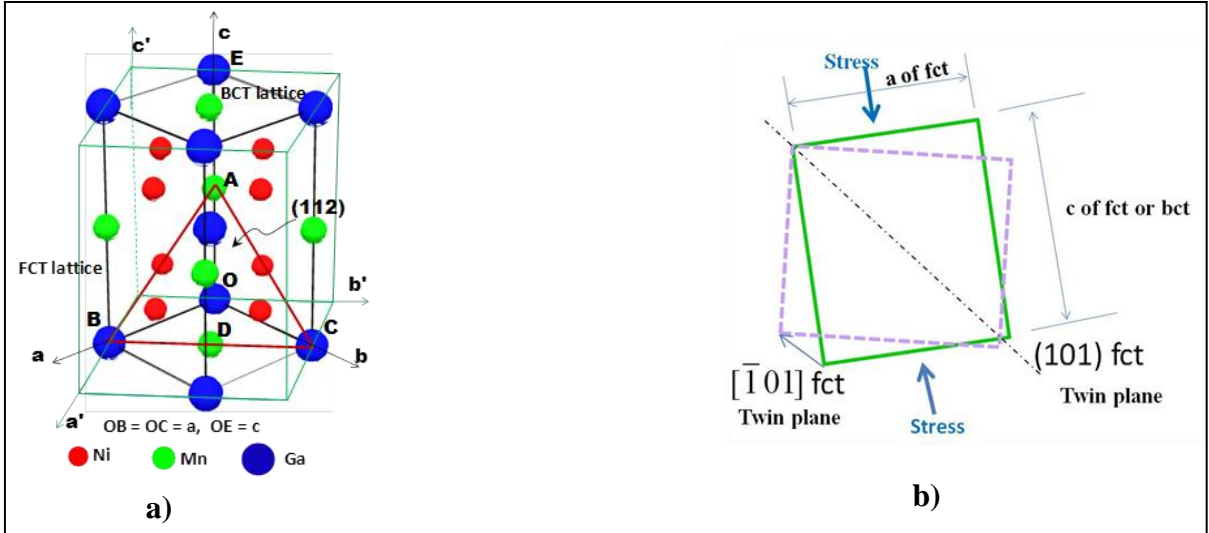


Figure 8. (a) Tetragonal lattice of bct martensite showing the location of Ni, Mn and Ga atoms. ABC is the (112) twin plane while AD is the [11-1] twin direction. The alternate fct representation is the skeleton shown by green lines, where it may be noted that the equivalent twin system is (101)[10-1]. The c/a ratio of the fct cell, that is in near orientation coincidence with the austenite lattice, is 1.18. The easy magnetization axis is [110] direction in the bct representation or [100] direction in fct description; note the location of Mn atoms that span the easy magnetization axis. (b) Sketch illustrating twin related transformation of the fct martensite unit cell under compressive load. The figure illustrates how a prior [001] direction rotates approximately by 90 degrees under compressive load, such that the easy magnetization [100] direction now aligns along the loading axis. The pole figures of figure 7 confirm this rotation.

4. Conclusions

It has been demonstrated that thermal cycling under compressive stress significantly enhances the MCE of polycrystalline $\text{Ni}_{2+x}\text{Mn}_{1-x}\text{Ga}$ alloys. Texture measurements using neutron diffraction have shown that thermal cycling leads to crystallographic alignment of the easy magnetization axis along the loading direction, and this then explains the MCE enhancement by up to 79%. Overall, a methodology for enhancing solid state magnetocaloric cooling has been established. This methodology will further facilitate Future Warfighter and Future Force application developments in self-powered personal and mobile magnetic cooling systems to enhance the Future Warfighter and Future Force capability.

5. References

1. Franco, V. et al. *Annu. Rev. Mater. Res.* **2012**, *42*, 305.

6. Transitions

Refereed Journal Paper:

- Giri, A. K.; Paterson, B.; McLeod, M. V.; Dennis, C. L.; Majumdar, B.; Cho, K. C.; Shull, R. D. Effect of Crystallographic Alignment on the Magnetocaloric Effect in Alloys Near the Ni₂MnGa Stoichiometry. *J. Appl. Phys.* **2013**, *113*, 17A907. doi: 10.1063/1.4793608
- McLeod, M. V.; Giri, A. K.; Paterson, B. A.; Dennis, C. L.; Shull, R. D.; Cho, K. C.; Majumdar, B. S. *Effects of Isobaric Thermal Cycling on Transformation Strains and Magnetocaloric Effect in Ni_{2+x}Mn_{1-x}Ga Alloys*; (Unpublished).
- Zhou, Le; Giri, Anit; Cho, Kyu; Heinrich, Helge; Majumdar, Bhaskar; Sohn, Yongho. *Microstructural and Crystallographic Characterization of Ni_{2+x}Mn_{1-x}Ga alloys (x=0.14, 0.16, 0.19, 0.22, and 0.24)*; (Unpublished).

Invited Talk:

- Giri, A. K.; Paterson, B.; McLeod, M. V.; Dennis, C. L.; Majumdar, B.; Cho, K. C.; Shull, R. D. *Magnetocaloric Effect in Grain Aligned Polycrystalline Ni_{2+x}Mn_{1-x}Ga Alloys*; College of Engineering, Florida International University, Miami, FL (Invited Seminar; October 12, 2012).
- Giri, A. K.; Paterson, B.; McLeod, M. V.; Dennis, C. L.; Majumdar, B.; Cho, K. C.; Shull, R. D. Crystallographic Alignment Effects on the Magnetocaloric Effect of near-Ni₂MnGa Alloys. *2013 TMS Annual Meeting & Exhibition*, March 3–7, 2013, San Antonio, TX (Invited Talk; March 5, 2013).
- Giri, Anit; Paterson, Brigitte; McLeod, Michael; Zhou, Le; Dennis, Cindi; Majumdar, Bhaskar; Sohn, Yongho; Cho, Kyu; Shull, Robert. *Enhanced Magnetocaloric Effect in Ni₂MnGa Based Magnetocaloric Alloys. Energy Materials Nanotechnology Fall Meeting (EMN Fall 2013)*; Orlando, FL, 7–10 December 2013 (Invited Talk; December 8, 2013).

Contributed Presentation:

- Giri, A. K.; Paterson, B.; McLeod, M. V.; Dennis, C. L.; Majumdar, B.; Cho, K. C.; Shull, R. D. Effect of Crystallographic Alignment on the Magnetocaloric Effect in Alloys Near the Ni₂MnGa Stoichiometry. *12th Joint MMM Intermag Conference*, Chicago, January 14–18, 2013 (Oral Presentation; January 17, 2013).
- McLeod, M. V.; Paterson, B.; Giri, A. K.; Zhou, L.; Dennis, C. L.; Cho, K. C.; Shull, R. D.; Sohn, Y. H.; Majumdar, B. S. Effects of Isobaric Thermal Cycling on Magnetocaloric Effect in Near Ni₂MnGa Alloys. *FSMA'13 - Fourth International Conference on*

Ferromagnetic Shape Memory Alloys, June 3–7, 2013, Boise, ID (Poster Presentation; June 6, 2013).

- Zhou, Le; Giri, Anit; Cho, Kyu; Sohn, Yongho. Martensitic Transformations Study from Composition Gradients Generated by Diffusion Couples for in NiMnGa System. *2014 TMS Annual Meeting & Exhibition*, San Diego, February 16–20, 2014 (Oral Presentation; February 19, 2014).
- McLeod, Michael; Giri, Anit; Zhou, Le; Vogel, Sven; Sohn, Yongho; Cho, Kyu; Majumdar, Bhaskar. Enhanced Magnetocaloric Effect (MCE) in Polycrystalline Ni₂MnGa Alloys Through Isobaric Thermal Cycling and Correlation with Texture Changes. *2014 TMS Annual Meeting & Exhibition*, San Diego, February 16–20, 2014 (Oral Presentation; February 19, 2014).

Briefing:

- Giri, Anit; Cho, Kyu. *Innovative Processing of Highly Efficient Rare Earth Free Magnetocaloric Materials*; Materials End of Year Review (January 25, 2013).
- Giri, Anit; Cho, Kyu. *Enhanced Magnetocaloric Effect in Ni₂MnGa Based Magnetocaloric Alloys*; Science Afternoon/MMSD Leadership meeting (April 2, 2013).

Thesis:

- Master's Thesis entitled "*Magnetocaloric Response of Ni_{2+x}Mn_{1-x}Ga Alloys and the Influence of Thermal Cycling Under Constant Stress*" New Mexico Institute of Mining and Technology, Materials & Metallurgical Engineering Department, Socorro, NM; Author: Michael McLeod; Advisor: Prof. Bhaskar Majumdar; Graduate Advisory Committee Member: Anit Giri (January 15, 2014)

Transition:

- A technology maturation level at the beginning of the current DRI effort entitled "Innovative Processing of Highly Efficient Rare Earth Free Magnetocaloric Materials" pertained fundamental scientific research to develop an original innovative processing technique to enhance magnetocaloric properties of rare earth free magnetocaloric materials was at technology readiness level (TRL) 1. Through the DRI research innovation efforts, the basic principles have begun to be formulated, validated, and applied toward Army specific applications with a target exit TRL 2. The only viable strategy to continue maturing the progresses of the current research innovation from beyond the low TRL post DRI to eventual technology transition for Army Warfighters applications is maturing through ARL WMRD S&T Mission program where a target exit TRL is 3. As such, a FY12-13 DRI Transition Plan to FY14-18 ARL WMRD Mission Program was proposed and submitted. It was not approved.

1 DEFENSE TECHNICAL
(PDF) INFORMATION CTR
DTIC OCA

1 DIRECTOR
(PDF) US ARMY RESEARCH LAB
IMAL HRA

1 DIRECTOR
(PDF) US ARMY RESEARCH LAB
RDRL CIO LL

1 GOVT PRINTG OFC
(PDF) A MALHOTRA

1 DIRECTOR
(PDF) US ARMY RESEARCH LAB
AMSRD ARL WM MB
A FRYDMAN

1 BENET LABS
(PDF) RDAR WSB L
E KATHE

3 DARPA
(PDF) J GOLDWASSER
M MAHER
N WIEDENMAN

2 US ARMY TACOM TARDEC
(PDF) SFAE GCS UA
C FILAR
J KOSHIKO

ABERDEEN PROVING GROUND

59 DIR USARL
(PDF) RDRL VTP
E CHIN
RDRL WM
P BAKER
B FORCH
S KARNA
RDRL WML
M ZOLTOSKI
RDRL WML A
W OBERLE
RDRL WML B
N TRIVEDI
B RICE
R PESCE-RODRIGUEZ
RDRL WML C
S AUBERT
RDRL WML D
R BEYER
RDRL WML E

P WIENACHT
RDRL WML F
M IIG
RDRL WML G
J SOUTH
RDRL WML H
J NEWILL
B SCHUSTER
RDRL WMM
J BEATTY
R DOWDING
J ZABINSKI
RDRL WMM A
J SANDS
J TZENG
E WETZEL
RDRL WMM B
T BOGETTI
B CHEESEMAN
C FOUNTZOULAS
G GAZONAS
D HOPKINS
T JENKINS
B LOVE
P MOY
B POWERS
C RANDOW
T SANO
R WILDMAN
C YEN
RDRL WMM C
J LA SCALA
RDRL WMM D
R CARTER
K CHO
A GIRI
M PEPI
S WALSH
RDRL WMM E
J SINGH
M COLE
J SWAB
J ADAMS
RDRL WMM F
H MAUPIN
S GREндаHL
L KECSKES
E KLIER
RDRL WMM G
A RAWLETT
RDRL WMP
D LYON
S SCHOENFELD
RDRL WMP A
R MUDD
RDRL WMP B

C HOPPEL
RDRL WMP C
T BJERKE
RDRL WMP D
J RUNYEON
RDRL WMP E
P SWOBODA
RDRL WMP F
N GNIAZDOWSKI
RDRL WMP G
N ELDREDGE

INTENTIONALLY LEFT BLANK.